Leibniz Universität Hannover

REDUCED PASSIVATION OF SILICON SURFACES AT LOW INJECTION DENSITIES CAUSED BY H-INDUCED DEFECTS

S. Steingrube[1], P.P. Altermatt[2], D. Zielke[1], F. Werner[1], J. Schmidt[1], and R. Brendel[1,2]
[1]Institute for Solar Energy Research Hamelin (ISFH) Am Ohrberg 1, 31860 Emmerthal, Germany
[2]Institute for Solid State Physics, Leibniz University Hanover, Appelstr. 2, 30167 Hanover, Germany
phone: +49(0)511 762 - 17253, fax: - 2904, steingrube@isfh.de

ABSTRACT: Surface recombination of Si solar cells is effectively reduced by deposition of charged dielectrics, such as positively charged SiN_x or negatively charged Al_2O_3. However, surface passivation of Si by positively charged SiN_x layers is well known to deteriorate strongly at low illumination conditions for acceptor densities below 10^{17} cm^{-3}. Thus, the surfaces of *p*-Si cells are usually diffused with dopants. A qualitatively similar effect has recently been observed for Al_2O_3 layers on *n*-Si. This phenomenon is not well understood and, accordingly, cannot be avoided up to date. We quantify this effect for all relevant dopant and injection densities by means of a physical model that includes a damaged region in a thin layer underneath the passivating layer. The thickness of this layer is 0.1 – 1 μm in case of SiN_x and only 10 – 100 nm for Al_2O_3. The damage does not necessarily originate from the deposition conditions alone, but possibly also from the wafer pretreatment. A tenfold improvement of the defect density within the surface damage region is shown to eliminate the problem.
Keywords: Recombination, Passivation, Modelling

1 INTRODUCTION

Recombination at surfaces of high-efficient laboratory silicon solar cells is efficiently suppressed using field effect passivation. Therefore, charged dielectrics, such as the positively charged amorphous silicon nitride layers (SiN_x, $Q_f \cong +2\text{x}10^{12}$ q/cm^{-2}) or Al_2O_3 ($Q_f = -$ (3-6)x10^{12} q/cm^{-2}), are deposited onto the Si surfaces. SiN_x has been established in the photovoltaics industry for many years, whereas Al_2O_3 is a current topic since it does not cause parasitic shunting when deposited onto the rear-side of *p*-type PERC silicon solar cells due to its negative charges [1].
However, measurements of the injection dependent effective carrier lifetime (τ_{eff}) of SiN_x–passivated non-diffused *p*-type silicon wafers have consistently shown that the surface passivation quality strongly deteriorates for excess carrier densities below $\Delta n = 10^{15}$ cm^{-3}. Since this poor performance is not observed above an acceptor dopant level of 10^{17} cm^{-3}, an additional high temperature process is typically applied to diffuse the surfaces with dopants. We recently observed that also Al_2O_3 deposited on *n*-Si does often perform not optimally at low illumination levels, qualitatively similar to the SiN_x behaviour on *p*-type substrates, but to a lesser extent.

Understanding the cause of the deteriorated passivation quality at low Δn might help to reduce costs in solar cell processing. For this reason, this paper aims at explaining possible reasons for this poor performance and suggests strategies to avoid it. We recently developed a highly predictive model to describe the measured injection dependent effective surface recombination velocity S_{eff} [2,3] of SiN_x–passivated surfaces. The model incorporates local lifetime reduction in regions near the surface as proposed by Refs. 4 and 5. In the current paper, we assume an exponential lifetime profile to reproduce S_{eff}-measurements of different field-effect passivating layers on *n*-Si and *p*-Si substrates using a consistent set of parameters. In particular, we investigate SiN_x layers deposited by direct plasma-enhanced chemical vapour deposition (PECVD), thermal atomic-layer-deposited Al_2O_3 (th-ALD), and Al_2O_3 deposited using plasma-assisted ALD (PA-ALD).

The model parameters are found by fitting the model via genetic algorithms to all available experimental data simultaneously.

2 APPROACH

The recombination velocity S at the surface is defined as the quotient of the recombination rate U_s and the excess carrier density Δn_s at the surface:

$$S = \frac{U_s}{\Delta n_s} . \quad (1)$$

Using Shockley-Read-Hall (SRH) theory, the recombination rate can be expressed as

$$U_s = \frac{n_s p_s - n_{i,eff}}{\dfrac{n_s + n_1}{S_p} + \dfrac{p_s + p_1}{S_n}} , \quad (2)$$

where

$$n_1 = N_c e^{\beta(E_d - E_c)}, \quad p_1 = N_v e^{\beta(E_v - E_d)} , \quad (3)$$

and the surface recombination parameters S_n, S_p are proportional to the defect density at the surface.
If charges or dopant-diffusions are present at the interface, the excess carrier densities Δn_s, Δp_s deviate from the excess carrier densities Δn=Δp, deep within the bulk. Since Δn_s and Δp_s are difficult to measure, Eq. (1) is usually replaced by the effective surface recombination velocity:

$$S_{eff,surf} = \frac{U_s}{\Delta n(z_{scr})} . \quad (4)$$

Here z_{scr} is the edge of the space charge region, where the energy-bands are flat.
To reduce the effective surface recombination velocity, two predominant mechanisms can be addressed. The first method accounts for a reduction of S_n, S_p by reducing the defect density at the surface which is typically achieved via saturation of dangling bonds with hydrogen. In the second approach, surface recombination is suppressed by

decreasing the product $n_s p_s$. A common way to achieve this is to deposit a dielectric layer onto the surfaces which forms a high fixed charge density Q_f close to the interface. As a consequence of the emerging band bending Φ_s at the c-Si interface, one carrier type is repelled from the surface while the other one is attracted by the charges. The requirement of charge neutrality in the whole device leads to the following implicit equation [6, 7] for Φ_s:

$$\frac{Q_f}{c} = p\left(e^{-\beta\phi_s} + \beta\phi_s - 1\right) + n\left(e^{\beta\phi_s} - \beta\phi_s - 1\right), \qquad (5)$$

where $c=2\varepsilon_0\varepsilon/(q\beta)$. In general, Eq. (5) needs to be solved numerically. However, in certain limiting cases, it reduces to a very simple expression. Assuming, *e.g.*, a high positive fixed charge density at the interface of a moderately doped silicon substrate, the density of electrons n_s dominates the density of holes p_s. Considering, in addition, low injection conditions, the band bending Φ_s at the surface is positive, and therefore Eq. (5) leads to the following approximation of S_{eff}:

$$S_{eff,surf} = S_p \frac{c}{Q_f^{\,2}} N_{dop} \propto N_{dop}\,. \qquad (6)$$

This means that for low injection conditions with $n_s >> p_s$, SRH-recombination at the surface predicts an injection independent behavior, where the absolute value of S_{eff} is proportional to the dopant density N_{dop}. Note that for $n_s << p_s$, S_{eff} is injection independent at low Δn, as well.

2.1 Various Interpretations of S_{eff} at Low Δn

S_{eff} cannot be measured directly, and instead, it has to be extracted from effective lifetime measurements. These measurements contain information only about the total recombination rate of the sample, which is the sum of both bulk- and surface-recombination:

$$\frac{1}{\tau_{eff}} = \frac{1}{\tau_s} + \frac{1}{\tau_b}\,. \qquad (7)$$

Therefore, a measured injection dependence of τ_{eff} may either be caused by an injection dependence of the bulk-lifetime τ_b or by an injection dependent surface-lifetime τ_s. An injection dependence of τ_b may be caused, for example, by strongly asymmetric capture cross section for electrons and holes. However, in case of high-quality FZ-wafers, the influence of bulk-recombination on τ_{eff} is negligible, and hence the injection dependence observed in the presented samples (Fig. 2) cannot be explained by an injection dependence of τ_b.

Assuming, in the following, the bulk-recombination to be known, we extract the effective surface recombination velocity S_{eff} of the symmetrically passivated samples (S_{front}=S_{rear}) using the approximate expression given by Sproul [8]:

$$S_{eff} = \frac{W}{2}\left[\tau_s - \frac{1}{D}\left(\frac{W}{\pi}\right)^2\right]^{-1}. \qquad (8)$$

Several suggestions to explain S_{eff} of SiN_x passivated surfaces have been published [9,10], but were partly revoked later [4].
Refs. 9 and 10 explain the injection dependence of S_{eff} at low Δn via a reduced band bending in the silicon bulk. This is either achieved via interface charges stored in the defect distributions at the interface which partly compensate the fixed insulator charge [1], or via an injection dependent insulator charge [2].
However, these assumptions were proven to be wrong [4] or inadequate to explain the injection dependence of highly passivating layers [3]. Instead, Refs. 4 and 5 suggest recombination in the space charge region as a possible cause, following a model for the SiO_2 interface [11]. We recently adapted this concept to explain the observed recombination on a microscopic level [2,3].
We remark that an injection dependent S_{eff} may also be caused by a spatially inhomogeneous charge density, as observed *e.g.* for Al_2O_3 [12]. However, our simulations show that very high charge fluctuations are required to observe a considerable effect: a variance near the measured charge density is necessary when assuming a Gaussian charge distribution across the surface.

2.2 The Surface Damage Region (SDR)

Based on the analytical approach, suggested in Refs. 4 and 5, we recently developed a more detailed physical model that allows us to deduce a microscopic interpretation [2,3]. Very high concentrations of hydrogen have been observed near the interface after wet chemical etching [19]. If hydrogen is present in intermediate concentrations at the interface, it is well known to saturate the silicon dangling bonds, and thereby contributes to the electronic passivation. Very high hydrogen concentrations may, however, cause lattice damage via interstitial hydrogen molecules, or form H-B or H-P complexes with the dopant atoms of the substrate, which may then act as traps.
In our microscopic model, we assume that there is a damaged region in the bulk near the interface, possibly caused by a high hydrogen density. Thereby, we assume that the volume density of defects is maximal at the interface and decreases exponentially into the bulk. Assuming the capture cross-sections to be independent of depth, this is equivalent to an exponential depth-profile of the SRH lifetime parameters $\tau_n(z)$ and $\tau_p(z)$, as shown in Fig. 1. They are truncated at the value of the bulk lifetime parameter τ_0:

$$\tau_n(z) = \min\left(\tau_{surf,n}\, e^{z/z_{\deg}}, \tau_0\right), \qquad (9)$$

$$\tau_p(z) = \min\left(\tau_{surf,p}\, e^{z/z_{\deg}}, \tau_0\right), \qquad (10)$$

where z_{deg} is the so called damage depth.

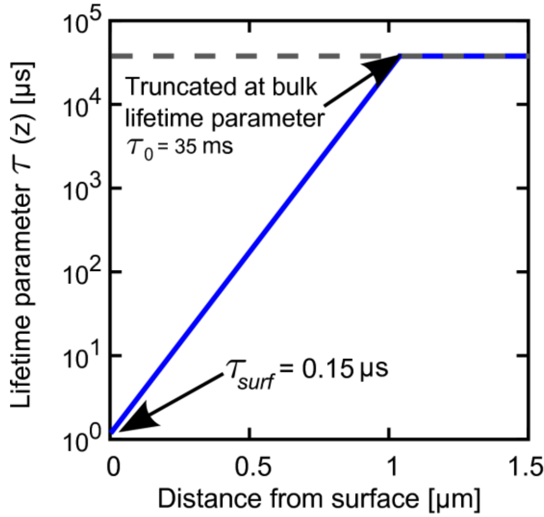

Figure 1: The lifetime-parameters $\tau_n(z)$ and $\tau_p(z)$ of the silicon bulk increase exponentially from the lifetime parameter at the interface, τ_{surf}, to the bulk lifetime parameter τ_b.

The reduced bulk-lifetime enhances S_{eff} by the additive term

$$S_{\deg} = \int_0^{z_{\deg}} U_{SRH}(z)\, dz / \Delta n \,, \qquad (11)$$

where U_{SRH} is the SRH recombination rate in the bulk.
In essence, S_{eff} has two main contributions: the usual interface recombination rate $S_{eff,surf}$, and the recombination rate in the surface damage region (SDR) S_{deg}. These two contributions are shown in Fig. 2 (c) for a *p*-type and an *n*-type substrate (1.5 Ωcm), passivated by a SiN_x layer. It is obvious that for low Δn, S_{eff} is dominated by recombination in the surface damage region, and at high Δn recombination via interface states is the predominant recombination path.

3 EXPERIMENTS AND MEASUREMENTS

The investigated silicon nitride films have a thickness of ≈ 70 nm [14]. They were deposited on both sides of the wafers in a high-frequency (13.56 MHz) direct PECVD reactor, with Ammonia and dilute silane (4.5% in nitrogen) used as the process gases [14]. The aluminium oxide films were fabricated via plasma-assisted (20 nm) ALD in an Oxford Instruments FlexAL™ reactor, or thermal ALD (30 nm). The process temperature of the SiN_x deposition is close to 400 °C, while the th-ALD samples are grown at 260 °C, and the PA-ALD samples are deposited at 200 °C. The as-deposited ALD-layers contain only a very low fixed charge density. During a subsequent annealing process at temperatures between 350 and 450 °C, a highly negative charge density is formed, which leads to the outstanding field-effect passivation properties of the Al_2O_3-layers.
The negative fixed charge density of the Al_2O_3 layers is determined by gradually depositing positive corona charges onto both sides of the samples, which partly compensate the fixed charges of the dielectrics. The deposited charges Q_C were quantified via Kelvin probe measurements. Transient lifetime measurements were performed after each Corona deposition. Flat-band conditions (full charge compensation) were then determined from the minimum of the τ_{eff} vs. Q_C graph (at $\Delta n = 10^{15}$ cm^{-3}). Assuming symmetric capture cross sections, the negative fixed charge density of the ALD-layers was determined to -5.2×10^{12} qcm^{-2} on *p*-type, and to -6.2×10^{12} qcm^{-2} on *n*-type material. In contrast, the positive fixed charge density of the SiN_x layers is approximately $+2.2\times10^{12}$ qcm^{-2} [2, 3].

4 NUMERICAL METHODS

The development of parametric models may contribute significantly to the improvement of solar cells if it relies on physically meaningful parameters, ideally obtained from independent experimental data. Thereby, the reliability of data fitting increases with the number of available data sets, and with the number of parameters that can be determined via independent experiments.
However, typically a large number of parameters remains undetermined during fitting, such as the exact values of τ_0, $\tau_{surf,p}$, $\tau_{surf,n}$, Q_f, S_n, S_p and z_{deg} for modeling the injection dependence of S_{eff}. During fitting, these parameters have to be carefully restricted to a physical meaningful range. Nevertheless, the number of local minima in the $N \times N$ parameter space increases rapidly with the number of free parameters *N*, which makes deterministic optimization procedures unsuitable.
Genetic algorithms meet the challenge of being insensitive to local minima and yet to converge relatively quickly. Such algorithms mirror biological evolution in which the fitness of a population is increased by the processes of selection, crossover, and mutation [15].
The fitting algorithm is initialized by setting a seed population. One or more parents are generated with an initial set of reliable parameter values. During each simulation step, a part of the population is replaced by newly generated children. In each step, the current population is evaluated using a fitness function that is based on the least-square-method. Only the "fittest" fraction of the population survives, and is able to propagate during the next simulation step. During propagation, children are generated by mixing the parameter values of two arbitrarily chosen parents, and adding a Gaussian noise to these parameter values. If the fitness of the fittest member of the population does not improve over several simulation steps, the Gaussian noise is reduced gradually to refine the fitting procedure close to the currently optimal parameter sets.
In the current work, we apply this algorithm to model the injection dependence of SiN_x and Al_2O_3 passivated *n*-type and *p*-type samples of various resistivities.
Fitting several samples simultaneously is important for the development of a consistent model. This is done as follows: several parameters can be assumed to be independent of the bulk resistivity and the passivating layer, and therefore, need to be optimized globally for all samples ("global parameters"). Some parameters, however, depend on the bulk-doping or the deposited material, and thus, need be varied freely during fitting ("local parameters").
We developed a special fitting algorithm, which allows to adjust global and local optimization parameters

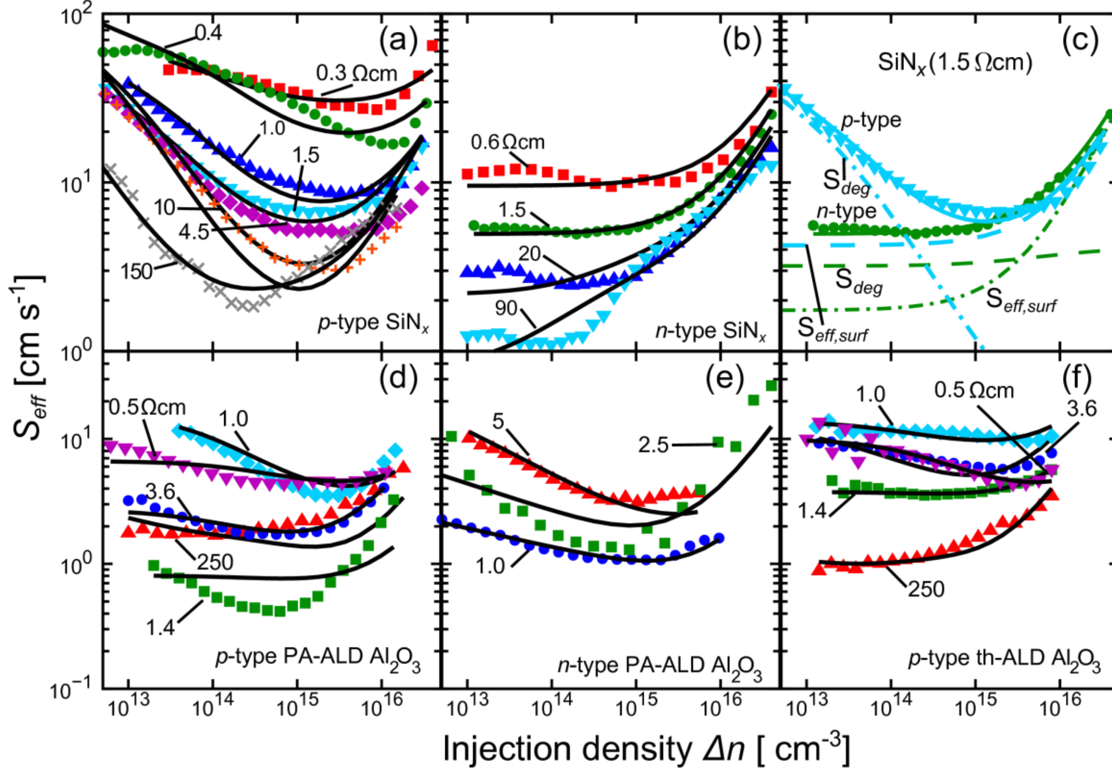

Figure 2: Measurements (symbols) of the injection dependent S_{eff} behavior of *n*-type and *p*-type substrates with various resistivities, passivated using (a) and (b) direct PECVD-SiN_x [14], (d) and (e) plasma-assisted ALD Al_2O_3, and (f) thermally grown ALD Al_2O_3. The S_{eff} values are extracted from transient τ_{eff} measurements using Eqs. (7) and (8). The bulk-lifetime is calculated using SRH-theory with a SRH lifetime-parameter of τ_0=35 ms and applying the Auger parameterization of Kerr and Cuevas [16]. The simulated curves (lines) are obtained using the model of a surface damage region with the parameter sets displayed in Fig. 4. Please note the different scaling of the ordinate by two orders of magnitude between top and bottom graphs, which shows that the SDR effect has rather negligible influence in case of Al_2O_3. (c) Resolving S_{eff} into its additive contributions - surface recombination (S_{it}) and recombination in the SDR (S_{deg}) - shows that S_{deg} clearly dominates the total recombination rate at low Δn as well on SiN_x–passivated *n*-type as also on *p*-type substrate

simultaneously, automatically, and very reliably for an arbitrary large set of measurements.

In this particular case, the fitness function f used to evaluate a parameter set for the genetic optimization algorithm, is defined as the weighted sum of the average square deviation between measured data points and simulated curves, and the average square distance of the derivative of simulated and experimental curves, which is done to approximate the curve characteristics:

$$f = \frac{1}{M-1}\left(\omega_x \sum_{i=1..M} (\Delta_x)^2 + \omega_{\partial x} \sum_{i=1..M} (\Delta_{\partial x})^2 \right), \qquad (12)$$

where M is the number of data points of the S_{eff} measurement.

4. RESULTS

4.1. Fit Results and Discussion

The 24 available data sets of SiN_x and ALD-passivated substrates of different bulk resistivity (*n*-type and *p*-type) are fitted simultaneously using the surface damage model. Thereby, a consistent set of physical meaningful parameter values is obtained (Figure 3). In particular, only two parameters need to be treated as local parameters: the damage depth z_{deg} and the surface recombination velocity parameter $S_n = S_p := S_0$. The reduced surface lifetime-parameter for electrons $\tau_{surf,n}$ is optimized globally to 0.15 µs. Since it may be assumed that the ratio of the capture-cross sections for electrons and holes differs for *n*-type and *p*-type substrates, a discrimination between dopant type is made, here. We find $\tau_{surf,n}/\tau_{surf,p} = 4 \times 10^{-3}$ on *p*-Si, and $\tau_{surf,n}/\tau_{surf,p} = 9.55 \times 10^{-3}$ on *n*-Si. The fixed charge density of the ALD layers is taken from measurements (Sec. 3), and Q_f for SiN_x layers is fixed to $+2.21\times10^{12}$ q/cm^{-2} [2,3].

Figure 3 shows that S_0 scatters in a range between 2×10^3 and 3×10^4 cm/s, and no clearly visible doping dependence is visible. This is not surprising, since S_0 is the only remaining free parameter to adjust the position of the S_{eff} curves. Slight differences in the charge density may, for example, cause considerable changes in the fitted S_0-value. In addition, the limitations of experimental reproducibility may indeed lead to a scattering of the interface defect density which is proportional to S_0. Examples of critical processing steps are the exact deposition- and temper- conditions and the chemical wafer pretreatment.

For most passivating layers, we find a clear decrease of

the damage depth z_{deg} with N_{dop}. Interestingly, we also find a strongly reduced value of z_{deg} in case of th-ALD and PA-ALD (10 – 100 nm) compared to the tenfold larger damage depths determined underneath SiN_x (0.1 – 1 µm) layers. This smaller extent of the SDR for Al_2O_3 causes a negligible reduction of the passivation quality at low Δn compared to the strong injection dependence of S_{eff} observed for SiN_x layers on *p*-type.

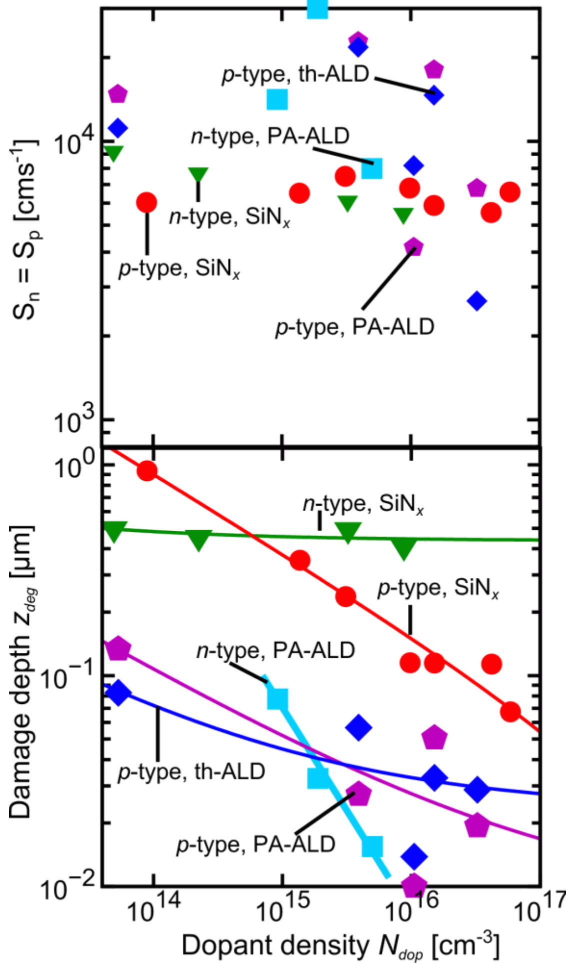

Figure 3: During fitting, the damage depth z_{deg} (bottom graph), and the surface recombination velocity parameter $S_n = S_p := S_0$ (top graph) are varied, in contrast to all remaining parameters, which are adjusted globally. The lines are guides to the eye. z_{deg} typically decreases with N_{dop}, and is by almost one order of magnitude smaller for ALD than for SiN_x. S_0 scatters considerably between 2×10^3 and 3×10^4 cm/s. The remaining parameters are fixed to $\tau_{surf,n} = 0.15$ µs, $\tau_{surf,n}/\tau_{surf,p} = 4 \times 10^{-3}$ (*p*-Si), and $\tau_{surf,n}/\tau_{surf,p} = 9.55 \times 10^{-3}$ (*n*-Si).

4.2 Understanding and Improving the Surface Damage

Because our model is physically sound, it allows us to predict which improvement of the lifetime in the degraded volume is necessary to maintain the high performance of a *p*-Si solar cell also at low illumination levels, even though it contains undiffused surfaces passivated with SiN_x. Note that for undiffused *n*-Si solar cells passivated using Al_2O_3 layers, the detrimental effect caused by the SDR is less pronounced, since the damage depth is by one order of magnitude smaller than for SiN_x. Figure 4 shows the S_{eff} values of a 0.4 Ωcm and of a 1.5 Ωcm sample, calculated using the $\tau_{surf,p}$ and $\tau_{surf,n}$ values that fit the experiments (continuous lines). For comparison, the S_{eff} values using τ_{surf} - values multiplied by a factor of ten are shown (dashed curves). Surprisingly, an improvement by a factor of mere 10 already avoids the unwanted S_{eff} behavior. A detailed understanding of the cause for the deteriorated region may help to achieve this improvement.

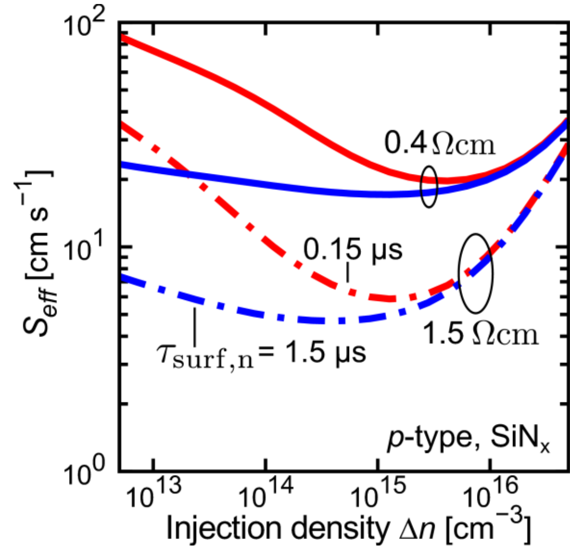

Figure 4: Calculated S_{eff} in the SiN_x passivated p-type Si samples with 0.4 Ωcm and 1.5 Ωcm resistivity. The continuous lines are determined using the values of $\tau_{surf,p}$ and $\tau_{surf,n}$ obtained from the fit. The dashed curves are obtained using enhanced values of τ_{surf}, multiplied by one order of magnitude. This shows that a strong improvement of S_{eff} towards low Δn can be achieved if the degradation lifetime parameters are increased by only a factor of ten.

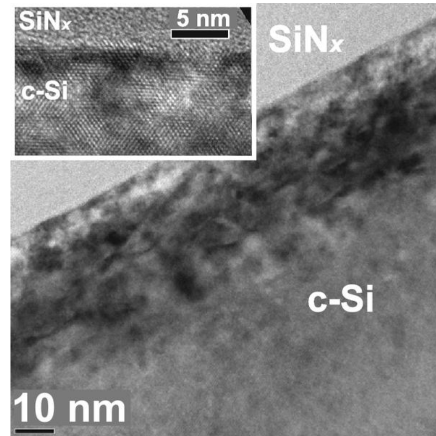

Figure 5: HRTEM images of a 30 nm thick defect-rich region in the Si substrate underneath a SiN_x passivating layer. Short, non-connected defect-like contrasts are observed that are aligned almost parallel to the interface.

4.3 Microscopic Explanation and Implications on Experiment

Our HRTEM images of the surface-near region underneath PECVD-SiN_x layers show defect-like contrasts reaching up to 30 nm into the Si substrate (Fig. 5.) This sample was deposited in a remote-plasma chamber (Oxford Instruments Plasmalab 80+) using silane and ammonia as process gases. A main cause for the formation of such a surface damage region underneath SiN_x layers might be the extremely high density of hydrogen (up to 10^{22} cm^{-3}) observed in Si substrates close to the SiN_x layer [13]. Such high densities of hydrogen in Si are known to lead to the formation platelets, and recombination-active deep-level defects [2, 3, 19, 20]. A possible source of hydrogen is the H stored in the SiN_x layers (typically 10–15 at. %). However, the H-content in the ALD-layers is only approximately 1 at. %. Therefore, we suggest that H-termination during wafer-pretreatment provides an additional, non-negligible source of hydrogen. H-termination during wet chemical etching is known to induce hydrogen in high concentrations into the Si wafer. This has been experimentally validated via acceptor deactivation close to the interface [19].

Further indications of hydrogen-related defects are obtained by comparing the penetration depth of hydrogen to the determined damage depth z_{deg}.

The effective diffusion coefficient D_{eff} of hydrogen in Si was experimentally determined by several groups (for an overview, see *e.g.* [17,18]) and is known to decrease from $D_{eff} \approx 10^{-11}$ cm^2s^{-1} at typical deposition temperatures of SiN_x (400°C) down to $D_{eff} \approx 10^{-12}$ cm^2s^{-1} at deposition temperatures of PA-ALD (200°C).

Assuming deposition times that are commonly reported in the literature (t = 2 − 10 min), the penetration depth $\sqrt{D_{eff}\, t}$ is roughly approximated to be 0.3−0.8 µm for SiN_x and 30-80 nm in case of PA-ALD. This estimation of the H-diffusion depth is exactly of the same order of magnitude as the depth of the surface damage region modeled in this work. In addition to a smaller diffusion coefficient, the out-diffusion of hydrogen during annealing of the Al_2O_3 layers may reduce the extent of the surface damage region further.

Our simulations predict that a moderate reduction of the H content will help to decrease recombination at low injection densities, while the good passivation properties at high illumination levels are maintained (Figure 4.).

5 SUMMARY AND CONCLUSION

The measured injection dependent effective recombination velocity S_{eff} of several silicon substrates which were passivated by three different high quality dielectrics (SiN_x, thermal ALD Al_2O_3, plasma-assisted ALD Al_2O_3) is quantified numerically. Recombination is described as the sum of two independent contributions: SRH-recombination at the surface, and SRH-recombination in a thin layer in the Si bulk underneath the surface where the lifetime is reduced [2,3]. Including this surface damage region (SDR) in the model, S_{eff} is reproduced to a high precision level in a wide range of excess carrier densities Δn and dopant densities, in both *p*-type and *n*-type Si.

The resulting extension of the damage layer is 0.1 – 1 µm underneath SiN_x, in contrast to only 10 – 100 nm underneath Al_2O_3-layers. The dependence of the lifetime reduction on the wafer doping and process temperature strongly suggests H-induced defects as the main cause for it [18]. An excessive amount of H (up to 10^{22} cm^{-3}) may be induced during substrate pretreatment and/or the deposition process [13]. We predict that reducing the amount of H to moderate levels improves surface passivation at low illumination conditions while still maintaining the good passivation properties at high illumination levels.

ACKNOWLEDGEMENTS

We are grateful for the preparation of the Al_2O_3 samples and lifetime measurements by M. Kessler, L. Vorspel, and B. Veith (ISFH). We also thank M. Seibt and A. Urban (University of Göttingen) for providing the HR-TEM images. Funding was provided by the State of Lower Saxony and the German Ministry for the Environment, Nature Conservation and Nuclear Safety (BMU) under contract number 0325050 (“ALD”).

References

[1] J. Schmidt, A. Merkle, R. Brendel, B. Hoex, M.C.M. van de Sanden, and W.M.M. Kessels, *Prog. Photovolt.* **16**, 461 (2008).

[2] S. Steingrube, P.P. Altermatt, D.S. Steingrube, J. Schmidt, and R. Brendel, *J. Appl. Phys.*, **108**, 014506 (2010).

[3] S. Steingrube, P. P. Altermatt, J. Schmidt, and R. Brendel, *Phys. Stat. Sol. RRL*, **4**, pp. 91-93 (2010).

[4] S. Dauwe, J. Schmidt, A. Metz, and R. Hezel, *Proc. 29th IEEE Photovoltaic Specialists Conf.*, New Orleans, LA, pp. 162–165 (2002).

[5] J. Schmidt, J. D. Moschner, J. Henze, S. Dauwe, and R. Hezel, *Proc. 19th European Photovoltaic Solar Energy Conf.*, Paris, France, WIP, Germany (2004).

[6] R. H. Kingston and S. F. Neustadter, *J. Appl. Phys.* **26**, pp. 718-720 (1955).

[7] A. S. Grove and D. J. Fitzgerald, *Solid-State Electron.* **9**, pp. 783-806 (1966).

[8] A. B. Sproul, *J. Appl. Phys.* **76**, pp. 2851-2854 (1994).

[9] J. R. Elmiger, R. Schieck, and M. Kunst, *J. Vac. Sci. Technol.* A **15**, 2418 (1997).

[10] J. Schmidt and A. G. Aberle, *J. Appl. Phys.* **85**, 3626 (1999).

[11] S. W. Glunz, D. Biro, S. Rein, and W. Warta, *J. Appl. Phys.* **86**, 683 (1999).

[12] J. M. Sturm, A. I. Zinine, H. Wormeester, and Bene Poelsema, *J. Appl. Phys.* **97**, 063709 (2005).

[13] B. Sopori, R. Reedy, K. Jones, Y. Yan, M. Al-Jassim, Y. Zhang, B. Bathey, and J. Kalejs, *Proc. 31st IEEE Photovoltaic Specialists Conf.*, Lake Buena Vista, Florida (2005).

[14] M. J. Kerr and A. Cuevas, *Semicond. Sci. Technol.* **17**, 166 (2002).

[15] M. F. Schubert, F. W. Mont, S. Chhajed, D. J. Poxson, J. K. Kim, and E. F. Schubert, *Optics Express* **16**(8), pp. 5290-5298 (2008).

[16] M. J. Kerr and A. Cuevas, *J. Appl. Phys.* **91**(4), pp. 2474-2480 (2002).
[17] R. Rizk, P. de Mierry, D. Ballutaud, and M. Aucouturier, *Phys. Rev. B* **44,** pp. 6141–6151 (1991).
[18] B. Sopori, Y. Zhang, R. Reedy, K. Jones, N. M. Ravindra, S. Rangan, and S. Ashok, *MRS Symposia Proceedings*, **719**, Materials Research Society, Pittsburgh, PA, pp. 125–131 (2002).
[19] J. Weber, *Phys. Status Solidi C* **5**, p. 535 (2008).
[20] N. M. Johnson, F. A. Ponce, R. A. Street, and R. J. Nemanich, *Phys. Rev. B* **35**, p. 4166 (1987).